ELSEVIER

Thermochimica Acta 330 (1999) 137–144

thermochimica acta

Temperature modulated DSC at intermediate-low temperatures

Patrick Mesquida*, Andrä le Coutre, Jan K. Krüger

Fachbereich 10.2 Experimentalphysik, Universität des Saarlandes, Geb. 38, 2.OG D-66123 Saarbrücken, Germany

Received 12 August 1998; accepted 7 December 1998

Abstract

In this paper we present a new cooling system for temperature modulated DSC (TMDSC) working down to about 60 K. In order to demonstrate the features of this new system in combination with commercial TMDSC apparatus, we present measurements of the specific heat capacity (c_p) around the phase transitions of betaine borate and betaine phosphate. For SilGel 604 we report c_p and sound velocity data around the melt, as well as around the glass transition.

Keywords: Temperature modulated DSC (TMDSC); Specific heat capacity; Glass transition

1. Introduction

Important applications for the method of differential scanning calorimetry (DSC) are studies of phase transitions and glass transitions in condensed matter. A significant improvement of this technique has been established by the application of temperature modulation to the conventional DSC method (TMDSC) now offering the possibility to perform quasi-isothermal measurements and to determine the complex specific heat capacity c_p^* [1–3]. Unfortunately, commercial TMDSC instruments suffer from their cooling equipments which seriously limits

1. the access of low temperatures,
2. the sensitivity of the measurements system, and
3. the operating time of a continuously running experiment.

Within this paper we propose a suitable cooling equipment which overcomes the above mentioned limitations. It has been adapted to two different commercial TMDSC apparatus maintaining the commercial calorimetric measurement systems (heaters, sensors, electronic equipment):

(a) Mettler-Toledo DSC821e,

(b) Thermal Analyst DSC2920-MDSC™.

Investigations of several phase and glass transitions will be presented in order to demonstrate the efficiency of the new cooling system.

2. Experimental

The most important requirements for the cooling system of a high performance TMDSC are: a stable thermal behaviour over a long period of time (constant temperature of the heat exchanger, homogenous temperature profile inside the cell, perfect decoupling of the heat exchanger from the environment, a low

*Corresponding author. Tel.: +681/302-3476; fax: +49-681-302-3443; e-mail: pame@stud.uni-sb.de

0040-6031/99/$ – see front matter
PII: S0040-6031(99)00028-3

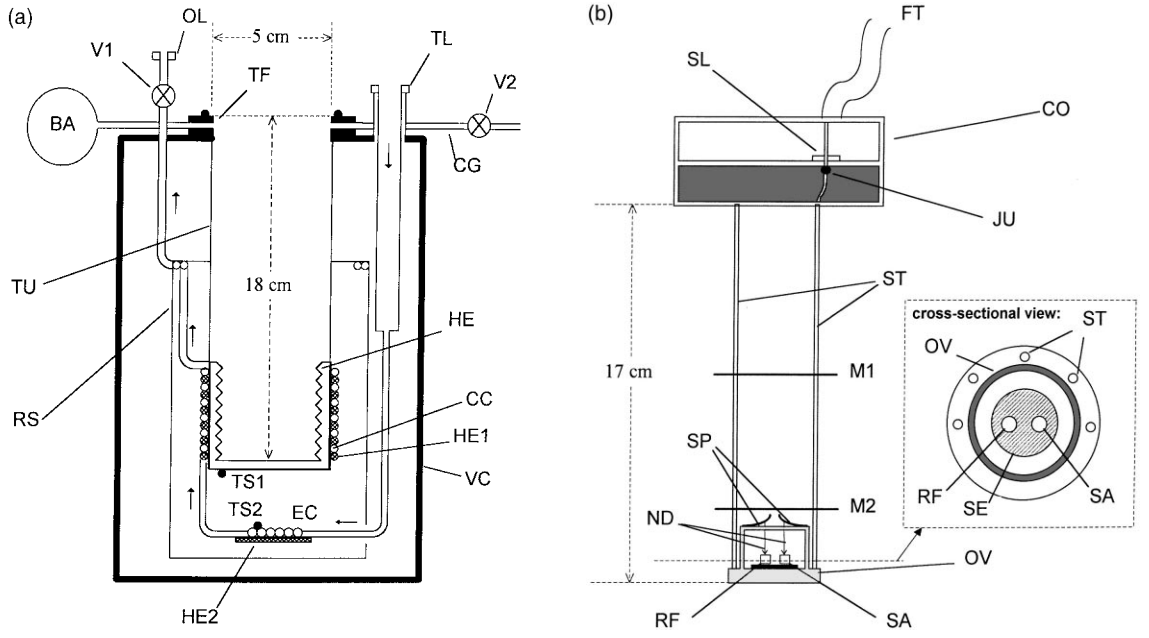

Fig. 1. (a) The thermostat/cryostat. OL=outlet, V1 and V2=needle valves, TF=top flange, TL=transfer line, CG=pipe for the contact gas, BA=balloon, TU=stainless steel tube, RS=radiation shield, HE=heat exchanger, CC=cooling coils, HE1=heating for HE, TS1=temperature sensor for HE, VC=vacuum chamber, EC=evaporation chamber, TS2=temperature sensor for EC, HE2=heating for EC. (b) The oven holder. FT=flexible metal tube, CO=cover, SL=sealed lead for the sensor wires, JU=junction and thermal compensation of the thermocouple wires, ST=thin stainless steel tubes, M1 and M2=metal discs, SP=plate springs, ND=steel needles, OV=DSC-oven, RF=reference pan, SA=sample pan, SE=DSC-sensor.

temperature noise level), prevention of contamination with moisture during the experiments, an expansion of the attainable temperature interval (especially to lower temperatures), a low consumption of coolant and the possibility to refill the coolant reservoir while an experiment is running.

The principles of the new thermostat/cryostat system are shown in Fig. 1(a) and (b). According to Fig. 1(a) and (b) the thermostat/cryostat is a top-loading system which consists of three main parts: the heat exchanger HE, the vacuum chamber VC and the top-loading holder of the oven (Fig. 1(b)), which is inserted into HE without having any direct mechanical contact with it. HE is connected through a thin-walled stainless steel tube TU with a diameter of about 5 cm to the top flange TF of the vacuum chamber VC. The cooling fluid is fed through the transfer line TL to an evaporation chamber EC. This chamber provides a mechanical and thermal decoupling from the heat exchanger. Prior experiences have shown that ''boiling'' of the coolant (especially in the case of nitrogen) in HE produces temperature fluctuations and acoustic noise thus reducing the accuracy of the measurements. In EC, the coolant is kept at a temperature slightly above its boiling point (using the heater HE2 and the temperature sensor TS2 connected to an external temperature controller) to keep constant the temperature of the cooling gas entering into HE (The influence of the thermal behaviour of a cryostat with and without an evaporation chamber on the oven temperature is shown in Fig. 2.) With the temperature sensor TS1 and with the heating wire HE1 winded parallel to the cooling coils CC around HE the temperature T_{HE} of HE can be actively controlled. The inside of HE has a ripple-enhanced surface in order to increase the heat transport to the even OV (Fig. 1(b)). Having passed HE the cooling fluid is used to pre-cool the radiation shield RS thus improving the decoupling from the laboratory.

The top loading holder (Fig. 1(b)) contains the DSC-oven OV. OV is suspended to the top cover CO with several small thin-walled stainless steel tubes

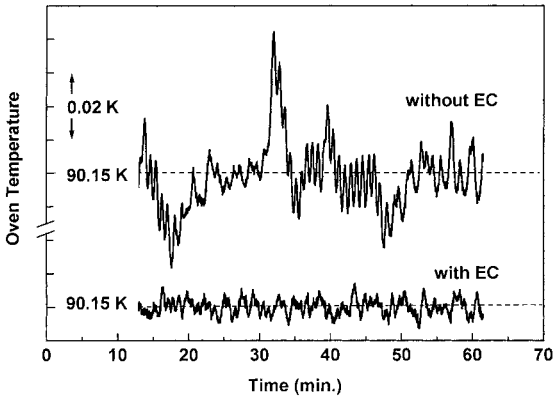

Fig. 2. Comparison of the oven behaviour with and without the evaporation chamber EC using nitrogen cooling. In both cases, the oven temperature has been set to 90.15 K. Upper curve: oven temperature vs. time without EC. Lower curve: oven temperature vs. time with EC (the temperature of EC has been set to 84.5 K).

ST. These tubes are used to feed the heating and sensor wires to OV. The thermocouple wires are thermally compensated by the junction JU inside CO and then guided through the sealed lead SL and the flexible metal tube FT to the electronical connectors of the TMDSC instrument. The metal discs M1 and M2 are used as convection and radiation shields. Inside OV lies the DSC-sensor SE with the sample and reference pans SA and RF which can easily be loaded by hand when the entire oven holder is lifted out of the cell by an external translation stage.

As shown in Fig. 1(b), the sample and reference pans SA and RF are pressed on the DSC-sensor SE by means of stainless steel needles ND with plate springs SP. This fixes the pans on the sensor plate and provides a well-defined seating and a good thermal contact of the pans on the sensors. Moreover, the measurements are now less sensitive to mechanical perturbances from outside.

The pipe CG (Fig. 1(a)) with the valve V2 serves as an inlet for the contact gas which provides a defined thermal coupling between HE and OV. Generally, we use He or N_2 as contact gas. During the measurements, the inner part of the heat exchanger cell is sealed by the cover CO and V2 is closed. Thus, the mass of the contact gas remains constant and by using the flexible balloon BA as a parallel reservoir, the gas pressure within HE is kept almost constant. As an important result, on any time-scale a contamination with moisture cannot occur.

There is almost no restriction for the type of cooling fluid. Cooling can be performed with cold gases like N_2 and He as well as with, for instance, cold liquids like pre-cooled methanol. A typical cooling set-up for N_2 or He cooling is shown in Bohn et al. [4]. A dewar contains liquid N_2 or He. The cold liquid is pumped through a transfer line to the heat exchanger of the TMDSC/DSC cell. Since the cold liquid is held at normal pressure, the dewar, if necessary, can be refilled during measurements by means of the refilling inlet. Particularly with the use of N_2, there is no restriction for the operating time. Consequently, TMDSC measurements can be performed on any time-scale required (see below). As a result of the vacuum insulation of all cold equipment, even measurements below 100 K did not consume more than 0.25 l N_2 per hour. Using He as a cooling gas and at the expanse of 0.7 l/h He, a temperature of 23 K at the sensor TS1 was brought about. Unfortunately, until now, the attainable temperatures for TMDSC measurements are limited to about 40 K by the controlling hard- and software of commercial equipments. Furthermore, the sensitivity of those sensors used in the majority of cases decreases rapidly at temperatures below 80 K. However, our new cooling system works satisfactorily in TMDSC mode down to about 60 K on the DSC821e apparatus [5]. The upper temperature limit of the heat exchanger is defined by the solders used and is estimated to be 850 K. Thus the heat exchanger does not limit the high temperature specifications of commercial TMDSC/DSC equipment. Due to this, further discussions will be focused on the low temperature properties of our new TMDSC thermostat/cryostat.

With N_2-cooling TMDSC measurements under quasi-isothermal conditions are possible down to about 90 K. Below that temperature, Helium has to be used as the coolant. An important feature for all DSC experiments at low temperatures is the highest possible cooling rate at a given temperature. Table 1 shows the attainable cooling rates with He: down to about 40 K a cooling rate of 16 K/min is possible. It is worth noting that heating runs can be performed much faster.

To illustrate the capabilities and the extended temperature range of the modified cooling system we

Table 1
Temperature modulated DSC at intermediate-low temperatures

Oven temperature (K)	Max. cooling rate (K/min)
430	52
298	26
130	17
70	16
37	16

show some results of specific heat capacity measurements.

3. Results and discussion

3.1. Betaine borate

Betaine borate ($(CH_3)_3NCH_2COO{\cdot}H_3BO_3$, BB) is a novel ferroelastic material of whose physical properties little is known about. This holds especially true for its thermal properties. Haussühl [6] reported a DTA analysis for the ferroelastic phase transition at $T_c \approx 142.5$ K, yielding a rough estimation of the excess specific heat of less than 0.02 J/g K. The transition is of second order and transforms the (orthorhombic) paraelastic phase into the low temperature (monoclinic) ferroelastic phase. The order parameter is the elastic strain component e_5 (Voigt's notation) [7,8] and the inverse susceptibility of the order parameter is therefore the elastic stiffness tensor component c_{55} reflecting a softening of a transversal acoustic mode by approaching T_c.

In Fig. 3 the specific heat capacity of betaine borate is plotted vs. temperature. The high temperature phase only shows a slight curvature within the $c_p(T)$ curve and the discontinuity of the excess specific heat was determined to be $\Delta c_p = 0.017$ J/g K at $T_c = 142.5$ K (high temperature onset). The noise amplitude of the c_p-data within this temperature range, as deduced from Fig. 3, appeared to be 0.003 J/g K (peak-to-peak noise). The agreement with a measurement of the dielectric constant on a crystal from the same source yielding $T_c = 141.6 \pm 0.6$ K [8] suggests an absolute temperature error of less than 1.5 K.

The total amount of time needed to perform this continuous measurement was about 12 h. According to our experience, commercial cooling units are not

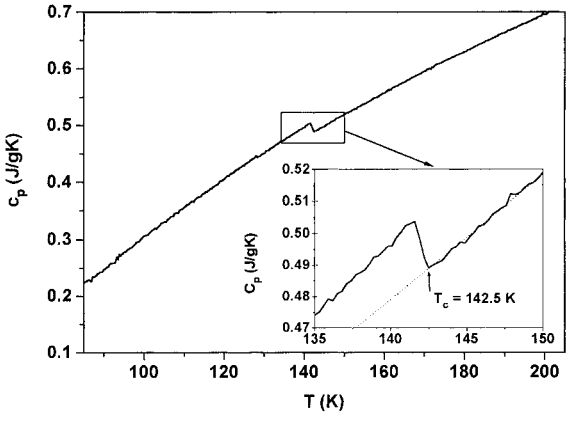

Fig. 3. Specific heat capacity (c_p) of betaine borate. Sample mass $m=21.71$ mg, without pans, amplitude and period of modulation $a=0.5$ K and $p=60$ s resp., underlying rate$=-0.15$ K/min; inset shows enlargement of rectangle at $T_c=142.5$ K.

able to yield the necessary stable thermal conditions during such a large operating time. It should be pointed out that a preliminary TMDSC measurement using a heat exchanger without the evaporation chamber EC on a sample of 3.59 mg in a aluminium pan did not show any evidence for the ferroelastic phase transition. Since the c_p-anomaly is known to be very small, the c_p-measurement was performed with a single crystal plate of larger mass ($m=21.71$ mg). In order to improve the detection sensitivity we have reduced undesired thermal resistances using neither a pan for the sample nor for the reference. The sample had a rectangular shape and polished surfaces. The thermal contact of the sample with the temperature sensor was improved using a steel needle preloaded with a plate spring (Fig. 1(b)) thus pressing the sample against the sensor plate. These measures, together with the new cryostat/thermostat system, offer the possibility to get the c_p-data of this small effect.

3.2. Betaine phosphate

On the one hand, in order to demonstrate the measurement capabilities of our new cooling equipment at intermediate-low temperatures, and on the other hand, to demonstrate the limits of the usual, commercial TMDSC method we have chosen betaine phosphate ($(CH_3)_3NCH_2COO\ H_3PO_4$, BP) as an example. BP undergoes an antiferrodistortive phase transition at $T_1=365$ K and an antiferroelectric phase

transition at $T_2 \approx 86$ K reported by Albers et al. [9]. A second low-temperature phase transition was detected by a study of the elastic properties of BP at $T_3 \approx 81$ K [10]. Maeda [11] performed specific heat measurements on a powder sample of 11.5 g yielding two small specific heat anomalies at $T_2 = 87.11$ K and $T_3 = 82.67$ K, respectively, consisting of two narrow peaks sitting on a weak but broadened excess background clearly deviating from the underlying linear $c_p(T)$ curve. Maeda [11] reports, for both subsequent transitions together, a small excess specific heat of $\Delta c_p < 7$ J/K mol (33 mJ/g K) and a transition entropy of 0.4 J/K mol (1.9 mJ/g K). According to Maeda [11] both low-temperature transitions are of second order.

Having extended the temperature range of our Mettler-Toledo DSC821e down to 60 K, these weak phase transitions were investigated with a modulation amplitude of 0.2 K, a period of 125 s and an underlying temperature ramp of −0.048 K/min. Helium was used both as the coolant and as the contact gas. In previous experiments, we found the sensitivity of commercial DSC sensors decreasing at lower temperatures thus making measurements of weak c_p-anomalies below 130 K difficult. With a simple of 17.06 mg contained in a standard aluminium pan we failed to detect the expected phase transitions at T_2 and T_3 with TMDSC. In order to increase the overall signal strength we used a heavier but flat monocrystalline sample plate of 43.54 mg. Moreover, to avoid undesired thermal resistances – as in the case of betaine borate – we did not use aluminium pans either on the sample or on the reference side of the sensor plate. Taking these precautions into account, we found both low-temperature transitions ($T_2 = 86.3$ K and $T_3 = 81.8$ K) close (within the same error margin as in the case of BB) to the temperatures reported in [11]. Representative for both low-temperature transitions, Fig. 4 shows the modulated heat flow as a function of time around the transition at T_3. The transition appears as an extremely sharp spike on the modulated heat flow signal, the latter representing the background heat capacity. Taking into account the above mentioned modulation time and amplitude the transition spikes appear in a temperature interval smaller than 0.05 K. This sharpness of the transition peaks suggests that the related transition is of first order rather than that of second order. After separation of the peaks

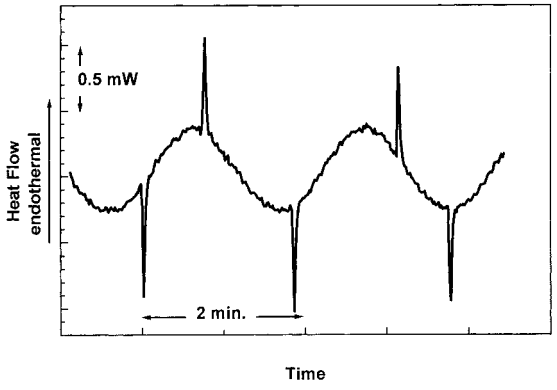

Fig. 4. Modulated heat flow of betaine phosphate vs. time. Parameters: sample mass $m = 43.54$ mg, without pans, modulation amplitude $a = 0.2$ K, modulation period $p = 125$ s, underlying rate $r = -0.048$ K/min.

from the sinusoidal heat flow signal, its amplitude shows only a linear temperature dependence without any additional contribution of the excess specific heat as reported by Maeda. Integrating over the heat flow peaks yields transition entropies of $\Delta s_3 = 0.27 \pm 0.04$ mJ/g K for the transition at T_3 and $\Delta s_2 = 0.24 \pm 0.03$ mJ/g K for the transition at T_2. For this purpose the heat flow has been calibrated at $T = 90$ K by using the background c_p of Maeda [11] measured by adiabatic calorimetry.

To calculate c_p-data from the modulated heat flow signal, the TMDSC algorithm uses one frequency component of the Fourier transform [1]. With this treatment one tries to describe the measured heat flow data by a single sinusoidal function, which seems not to be an appropriate data treatment for this case. Because the phase transformation peaks are narrow (Fig. 4) in comparison to the sinusoidal modulation period, this method provides an inadequate approximation to the raw data. However, we have tentatively applied the standard TMDSC analysis to our modulated heat flow data yielding the result given in Fig. 5. As expected, this analysis failed in the immediate vicinity of the phase transformations. One sees that the transition peaks appear to be much broader than in the original heat flow data. At higher or lower temperatures, or between the two peaks, where the heat flow signal is purely sinusoidal, the TMDSC analysis undoubtedly yields correct c_p-data. In contrast to [11] we found no excess specific heat contribution in these regions.

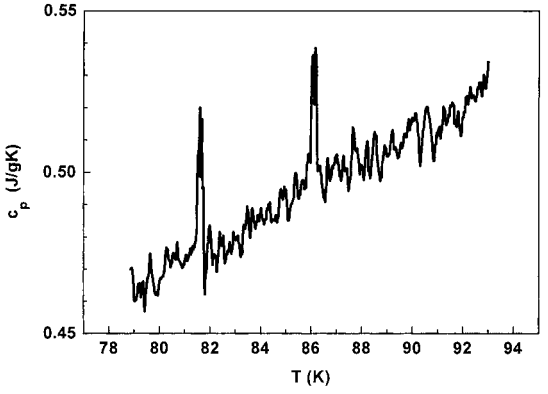

Fig. 5. Specific heat capacity (c_p) of betaine phosphate. Parameters: see Fig. 4.

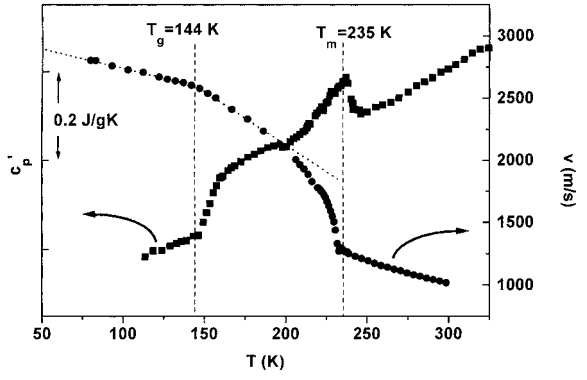

Fig. 6. SilGel 604. Real part of the complex specific heat capacity (c_p', left axis) measured by time domain TMDSC and longitudinal hypersonic velocity (v, right axis) measured by Brillouin spectroscopy vs. temperature. Time domain TMDSC (quasi-isothermal modulation), sample mass m=22 mg, standard Al-pans, temperature amplitude a=0.5 K, period p=60 s. Distance between two temperature steps depending on temperature region (1 K in the vicinity of the transitions; 5 K in the liquid state). Different measurement times for a single point (from 30 min up to 12 h depending on T). T_g: operative thermal glass transition temperature, t_m: upper temperature limit of the melting process.

3.3. SilGel 604

SilGel 604 is a standard silicon rubber of the RTV-2 group produced by the WACKER Chemie, München. SilGel 604 is a highly transparent silicon rubber which is made by addition-vulcanisation from the two parent products. Although the vulcanized SilGel 604 does still crystallize, due to the chemical network formed during the vulcanisation process this crystallisation is never fully complete therefore implying that there exists a maximum crystallinity which is well below 100%. The remaining amorphous matrix necessarily undergoes a thermal glass transition at a temperature T_g which is well below the equilibrium melting temperature T_m.

The goal of the present investigation was twofold: we were interested (i) in the thermal behaviour of the melt and the glass transition of SilGel 604 in the limit of an extremely low effective heating rate, and (ii) in the question where the thermal and the acoustic transition anomalies of this material coincide.

In order to clarify question (i) we performed time domain TMDSC measurements [4,12] after having slowly cooled down the sample to about 100 K, making sure that the sample did no longer adhere to the sample pan. Thus, the heating run shown in Fig. 6 (squares) was essentially performed on a mechanically free sample. Each data point was measured within the time domain, which means that after each temperature change a TMDSC measurement was made as a function of time always awaiting a constant heat flow signal level and therefore measuring equilibrium properties. The measurement of the complete heat capacity curve shown in Fig. 6 took 14 days, yielding an effective heating rate of 0.01 K/min (heating from 100 to 330 K). If the calibration procedure is not performed with a very sample-like calibration substance, the maximum error of the absolute c_p-values at $T \approx 100$ K may be as large as 25%. Nevertheless, the statistical error is minimised by the isothermal measurements. For comparison we have performed high resolution Brillouin scattering investigations (BS) over a wide temperature range (Fig. 6, circles). The BS technique measures hypersound frequencies (in this case≈5 GHz) of thermal phonons with a specified wave vector and has been reported elsewhere [13].

As usual, the glass transition is reflected by a kink in the sound velocity curve corresponding to the thermal glass transition of SilGel 604. A least square fit of two linear segments with a free running point of intersection (dotted line in Fig. 6) yielded the temperature T_g=144 K. The step-like c_p'-anomaly of the glass transition appears to be rather sharp and displays the onset of the excess specific heat at T_g. It is obvious that T_g corresponds to the onset temperature of the excess specific heat and is not at all correlated to the

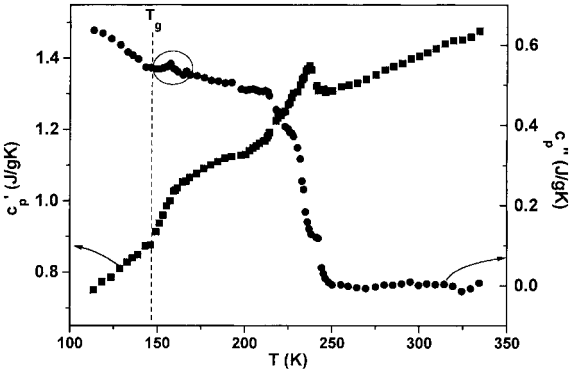

Fig. 7. Real (c'_p, left axis) and imaginary (c''_p, right axis) part of the specific heat capacity of SilGel 604 vs. temperature. Parameters: see Fig. 6.

inflection point (at T=152 K) of the specific heat curve which is about 8 K above T_g. It is worth noting that because of the extremely high probe frequency of BS the elastic data reflect the mechanically clamped state. Therefore, at T_g, BS measures static properties and the sound velocity data are not masked by relaxation effects.

The melt transition is spread over an interval from ≈200 to ≈235 K showing an almost 'lambda-like' increase of the excess specific heat capacity Δc_p (≈0.1 J/g K). At the beginning of the melting process the sound velocity deviates from the linear temperature dependence between T_g and T≈200 K. Furthermore, it results in a strongly bend sound velocity curve showing a drastic change in slope at the end of the melting process.

We have also tried to get some information from the imaginary part c^*_p of the complex specific heat capacity c'_p (Fig. 7). Keeping in mind that the measured phase angle shift is also influenced by changes of c'_p, we have calibrated the physical phase angle by taking the measured phase angle of the liquid phase as the instrumental one and setting it to zero. The melting of SilGel 604 is accompanied by a steep decrease of c''_p. At T_g the quantity c''_p shows a clear kink. Whether in addition there is a small α-relaxation peak (circle in Fig. 7) is not yet clear.

These results seem to support our general understanding of the thermal glass transition in the sense that there exists an inherent glass transition at a well specified transition temperature behind the operative glass transition masked by kinetic events [14–17].

4. Summary

We presented a new thermostat/cryostat system which has been adapted to commercial TMDSC instruments. To demonstrate the performance of the cooling system, experimental results of specific heat capacity measurements have been shown. The temperature interval of the commercial apparatus has been significantly expanded to lower temperatures allowing measurements on phase and glass transitions down to about 60 K. The stability of the thermal environment has been improved drastically to make possible quasi-isothermal TMDSC experiments which usually require long running times without interruption of the measurement. Moreover, the results of TMDSC and Brillouin spectroscopy measurements presented in this paper are helpful for a better understanding of the nature of the glass transition.

Acknowledgements

We express our thanks to Mettler-Toledo who have supplied us a complete type DSC821e instrument. TA-Instruments is acknowledged for providing a special DSC oven. Special thanks go to Prof. Dr. H.G. Unruh and Dr. A. Klöpperpieper (Univ. des Saarlandes) for providing us the betaine borate and betaine phosphate samples. This work was partly supported by the Sonderforschungsbereich 277.

References

[1] A. Boller, Y. Jin, B. Wunderlich, J. Therm. Anal. 42 (1994) 307.
[2] M. Reading, B.K. Hahn, G.S. Crowe, US Patent no. 5 224 775, 6 July 1993.
[3] M. Reading, D. Elliot, V.L. Hill, J. Therm. Anal. 40 (1993) 9314.
[4] K.-P. Bohn, A. Prahm, J. Petersson, J.K. Krüger, Thermochim. Acta 304/305 (1997) 283.
[5] P. Mesquida, Diploma Thesis, Universität des Saarlandes, Saarbrücken, 1998.
[6] S. Haussühl, Solid State Commun. 50 (1984) 63.
[7] K. Aizu, J. Phys. Soc. Jpn. 28 (1970) 706.
[8] H.G. Zimmer, Th. Hermann, H.-G. Unruh, Zeitschrift f. Phys. B 99 (1996) 245.
[9] J. Albers, A. Klöpperpieper, H.J. Rother, K.H. Ehses, Phys. Stat. Sol. (a) 74 (1982) 553.

[10] M. Maeda, J. Phys. Soc. Jpn. 57 (1988) 3059.
[11] M. Maeda, T. Atake, Y. Saito, H. Terauchi, J. Phys. Soc. Jpn. 58 (1989) 1135.
[12] J.K. Krüger, R. Jiménez, K.-P. Bohn, C. Fischer, Phys. Rev. B 56(14) (1997) 8683.
[13] J.K. Krüger, in: H. Bässler (Ed.), Brillouin Spectroscopy and its Application to Polymers in Optical Techniques to Characterize Polymer Systems, Elsevier, Amsterdam, 1989.
[14] J.K. Krüger, K.-P. Bohn, R. Jiménez, Condensed Matter News 5 (1996) 10.
[15] J.K. Krüger, K.-P. Bohn, R. Jiménez, J. Schreiber, Colloid Polym. Sci. 274 (1996) 490.
[16] J.K. Krüger, K.-P. Bohn, J. Schreiber, J. Phys. Condensed Matter 8 (1996) 10863.
[17] J.K. Krüger, K.-P. Bohn, J. Schreiber, Phys. Rev. B 54 (1996) 15767.